Bone 200 (2025) 117595

Contents lists available at ScienceDirect

Bone

journal homepage: www.elsevier.com/locate/bone

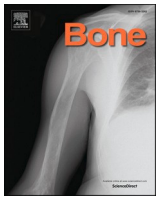

Full Length Article

How vascularization is reciprocally coupled to chondrogenesis and osteogenesis in bone healing: lessons from the growth plate

Julia Mehl [a,b,c], Katharina Schmidt-Bleek [a,b], Agnes Ellinghaus [a,b], Stefan Mundlos [b], Holger Gerhardt [d,e], Georg N. Duda [a,b,*], Viola Vogel [c,**]

[a] Julius Wolff Institute, Berlin Institute of Health at Charité - Universitätsmedizin Berlin, Germany
[b] Berlin Institute of Health Center for Regenerative Therapies, Berlin Institute of Health at Charité - Universitätsmedizin Berlin, Germany
[c] Laboratory of Applied Mechanobiology, Department of Health Sciences and Technology, ETH Zurich, Switzerland
[d] Max-Delbrück-Center for Molecular Medicine (MDC) in the Helmholtz Association, Berlin, Germany
[e] German Center for Cardiovascular Research (DZHK), Partnersite Berlin, Germany

ARTICLE INFO

Keywords:
Bone healing
Chondrogenesis
Vascularization
Mechanobiology

ABSTRACT

Despite considerable progress, the underlying mechanisms that enable scar-free regeneration in bone after injury are still not well understood. Here, we compared the spatiotemporal distribution of SOX9-positive chondrocytes, SPARC-positive hypertrophic chondrocytes and osteoblasts, versus Osterix-positive osteoblasts, i.e. key cell types in cartilage and bone formation, in the fracture gap of a mouse osteotomy model with the orderly sequence of events observed in the growth plate. We show that external mechanical stability determines the spatial distribution of osteoblastic and chondrogenic cell populations at day 7, thus defining the site of chondrogenesis initiation. At day 14, only rigid, but not semi-rigid fixation promoted the formation of avascular regions within previously vascularized areas. We thus propose a model how mechanical stabilization promotes bone healing: Blood vessel growth into the hematoma is followed by localized vascular degradation as chondrogenesis progresses, ultimately leading to vascular regrowth via endochondral ossification initiated at the tips of the distal bones. Deepening our understanding of these processes and how they ultimately relate to scar-free bone regeneration is of significant medical relevance as they can provide instructions how to promote fracture healing.

1. Introduction

Endochondral ossification follows a linear sequence of cellular differentiation events at the growth plate during bone growth. The resting zone, positioned at the top of the growth plate near the epiphysis, functions as a niche for skeletal stem cells [1,2]. It transitions into the proliferative zone, where chondrocytes organize into columns, aligning parallel to the long bone's longitudinal axis [3–5]. The process is highly organized: proliferating chondrocytes polarize perpendicular to the long bone axis [6], then enlarge as oxygen levels decline, ultimately reaching their maximum size in the hypertrophic zone [7]. Contrary to previous beliefs that hypertrophic chondrocytes undergo apoptosis, recent data showed that hypertrophic chondrocytes have the ability to transdifferentiate into osteoblasts, thereby initiating the process of endochondral bone formation [8–11]. Throughout these well-orchestrated stages, chondrocytes exhibit a distinct pattern of extracellular matrix (ECM) secretion that changes with their stage of maturation. While chondrocytes synthesize collagen II, with the highest expression observed in the lower proliferative and pre-hypertrophic zones [12], chondrocytes in the terminal hypertrophic zone situated near the metaphysis deposit collagen X [13].

Besides facilitating longitudinal growth in long bones at the growth plate, endochondral ossification also occurs during bone fracture healing, which typically proceeds through a cartilaginous phase [14]. However, while endochondral ossification at the growth plate progresses within a highly organized cartilage template established during skeletal development, fracture healing begins within a hematoma populated by inflammatory cells and a heterogeneous mix of progenitor cells. Before endochondral ossification can begin within the fracture gap, the hematoma must undergo a complex remodeling process

* Correspondence to: G. Duda, Julius Wolff Institute and Berlin Institute of Health Center for Regenerative Therapies, Berlin Institute of Health at Charité - Universitätsmedizin Berlin, Berlin 13353, Germany.
** Correspondence to: V. Vogel, Laboratory of Applied Mechanobiology, Department of Health Sciences and Technology, ETH Zurich, Zurich 8006, Switzerland.
E-mail addresses: georg.duda@charite.de (G.N. Duda), viola.vogel@hest.ethz.ch (V. Vogel).

https://doi.org/10.1016/j.bone.2025.117595
Received 25 May 2025; Received in revised form 16 July 2025; Accepted 16 July 2025
Available online 29 July 2025

characterized by inflammatory resolution, vascular invasion, and matrix reorganization, ultimately leading to cartilage and bone formation. A critical step in this remodeling is the invasion of blood vessels into the hematoma, which occurs alongside the pro-inflammatory and anti-inflammatory phases of healing [14]. Angiogenesis during fracture repair is highly mechanosensitive, with vascular sprouting into the hematoma strongly influenced by physical and mechanical cues [15–18]. Notably, the mechanical stability of fracture fixation exerts a greater influence on vascular self-organization than endothelial mechanotransduction processes mediated by the mechanosensitive transcriptional co-activators YAP and TAZ [19]. While vascular patterning within the fracture gap, directed by external mechanical stability, plays a crucial role in shaping the local microenvironment, it remains unclear how vascular organization influences the differentiation of competing cell populations and, consequently, the spatial patterning of cell populations during fracture repair. In addition to guiding vascular patterning, mechanical stability is well established as a major determinant of the overall rate of fracture healing, beginning from the earliest stages of repair [20,21]. Insufficient mechanical stability can substantially delay or impair healing and, in severe cases, result in non-union [22,23]. Although increased interfragmentary movement is known to promote enhanced cartilage formation during repair [21,24], it remains unknown how mechanical stability influences the spatial initiation of chondrogenesis within the fracture gap. Furthermore, the mechanisms regulating spatiotemporal vascularization and its connection to chondrogenesis and subsequent endochondral ossification during fracture healing remain poorly understood.

The key transcription factors regulating chondrogenesis and ossification are Sry-related HMG-box 9 (SOX9) and Osterix (OSX), respectively. Together with its co-factors, SOX9 is essential for chondrocyte lineage specification [25,26], promotes collagen II expression [27], and suppresses cartilage vascularization [28]. As cartilage transitions to hypertrophy, the fraction of cells expressing SOX9 diminishes [28], and chondrocytes shift toward a pro-angiogenic state. This triggers the invasion of blood vessels at the cartilage-bone interface and facilitates the recruitment of OSX-expressing cells. OSX, in cooperation with runt-related transcription factor 2 (RUNX2), activates Col1a2 gene expression and drives osteoblast differentiation and bone formation by binding to osteoblast-specific gene promoters [29,30]. Importantly, SOX9 expression is regulated by hypoxia-inducible factor 1-alpha (HIF1α), leading to its upregulation in hypoxic regions [31], whereas OSX expression is closely associated with blood vessels and oxygen-rich environments [32,33]. While chondrocytes near the cartilage-bone interface downregulate SOX9 expression and transition from a proliferative to a hypertrophic state, they begin secreting the matricellular protein secreted protein acidic and rich in cysteine (SPARC), also known as osteonectin [34]. In addition to its expression in hypertrophic chondrocytes, SPARC is also expressed by osteoblasts, where it plays a critical role in bone maturation and mineralization by strongly binding to collagen I, hydroxyapatite, and other fibrillar collagens, including types II, III, and V [35–40]. While the sequential appearance and regulation of these markers during endochondral ossification at the growth plate are well characterized and highly structured, their temporal and spatial expression during fracture healing remains poorly understood.

In this study, we thus analyzed the spatiotemporal evolution of pre-chondrocyte and pre-osteoblast cell populations within the fracture callus and examined how their distribution correlates with local vascularization under varying mechanical stability conditions. Using a mouse osteotomy model, we selected two healing time points - day 7 and day 14 - to specifically capture the emergence of chondrogenic and osteoblastic cell populations (day 7) and the onset of endochondral bone formation (day 14), before the callus becomes predominantly remodeled into bone at later stages. To exploit our cellular markers as sensors to report on specific biochemical and biophysical niche properties in the fracture gap, we used the well-characterized and highly organized process of endochondral ossification in the growth plate as a reference. We stained for the transcription factor SOX9 to identify early chondrocyte differentiation and for the transcription factor OSX to detect pre-osteoblastic cells. Since SOX9 is no longer expressed by terminal hypertrophic chondrocytes, we additionally stained for the matricellular protein SPARC, which is expressed by both hypertrophic chondrocytes and osteoblasts [34,41], to specifically detect hypertrophic chondrocytes, particularly during the later stages of healing. To assess vascularization, we utilized the endothelial surface markers Endomucin (EMCN) and CD31, noting that CD31 is also expressed by platelets and monocytes [42,43]. Collagen fibers were visualized using label-free second harmonic generation (SHG) imaging, a nonlinear optical technique sensitive to the helical structure of collagen fibers. Notably, SHG signals arise primarily from collagen I fibers, but also from other isoforms, such as collagen III, which contributes to osteoblastogenesis [44,45]. Collagen II, which is predominantly found in cartilage, generates a comparatively weaker SHG signal as its fibrils are thinner and less tightly packed [46]. Using this approach, we aimed to determine the spatial and temporal initiation of chondrogenesis within the fracture callus leading to endochondral ossification and how these processes are coordinated with local vascularization during healing.

2. Results

2.1. SOX9 was expressed in the proliferative zone but decreased in the terminal hypertrophic zone of the growth plate

To investigate the cellular responses during endochondral ossification, we used 10-week-old female mice and analyzed the same femur to assess endochondral ossification at both the growth plate and the fracture gap (Fig. 1A). To provide a reference for subsequent analyses of bone healing, we first characterized chondrogenesis and endochondral ossification in the distal femoral growth plate, where these processes occur in a highly ordered and sequential manner. The growth plate facilitates bone elongation through a tightly regulated process of chondrocyte proliferation and hypertrophy, contributing to growth plate thickening [47–49]. While the resting zone contains small, disorganized chondrocytes, proliferating chondrocytes align into columns since the spatial confinement forces the cell division planes to align, thus creating stacks [50]. To evaluate chondrogenesis and the emergence of osteoblastic lineage cells, we assessed the expression of key regulatory markers across distinct growth plate zones. SOX9, a transcription factor essential for chondrocyte differentiation and collagen II expression, was abundantly expressed throughout the proliferative zone (Fig. 1B), as expected. In contrast, SOX9 expression markedly decreased in the terminal hypertrophic zone before the appearance of the SHG-positive collagen I/III-rich region, which is marked by the white dashed line in the immunofluorescence image (Fig. 1B). This decrease of SOX9 expression coincided with the onset of vascular invasion as illustrated in the intensity profile plot along the cartilage-bone transition zone. The black dashed line in the plot corresponds to the same transition zone marked by the vertical dashed line in the image (Fig. 1B). This finding is consistent with previous reports showing that SOX9 suppresses cartilage vascularization [28,51].

2.2. SOX9 and SPARC were both expressed in the hypertrophic zone of the growth plate

To further identify the appearance of hypertrophic chondrocytes in the growth plate, we probed for SPARC expression. SPARC expression was first detected in the hypertrophic zone, in regions that still contained abundant SOX9-positive cells. As expected, SPARC expression continued into the mineralized region toward the metaphysis (Fig. 1C), where SPARC plays a critical role in initiating and promoting matrix mineralization [35–39]. Thus, this suggests that within the hypertrophic zone, either two distinct cell populations co-exist, one expressing SPARC and the other SOX9, or that cells in this transition region co-express

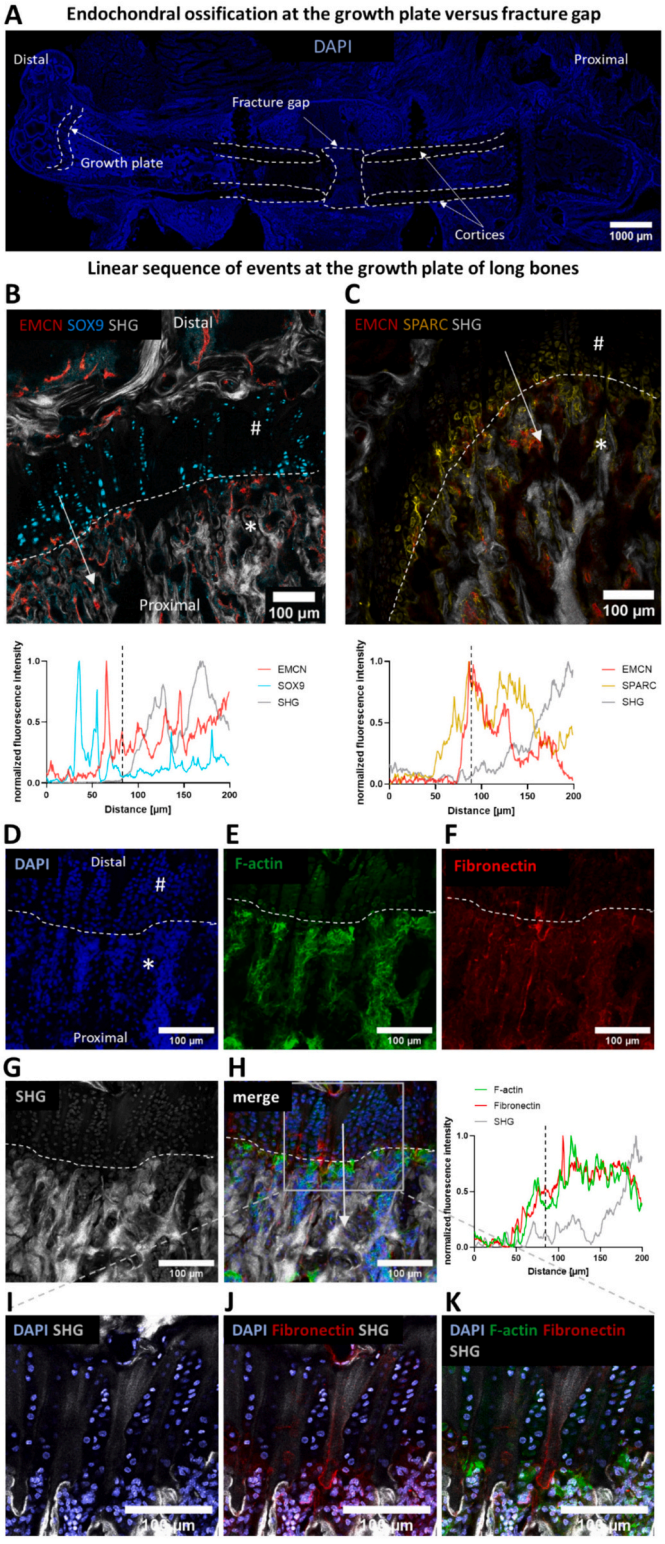

(caption on next column)

Fig. 1. Spatiotemporal shifts of cell populations during classical chondrogenesis and endochondral ossification in the growth plate of long bones. A. Representative overview image of the whole femur of 10-week-old female mice, 14 days post-osteotomy under semi-rigid fixation, stained with DAPI for nuclei. B. Spatial distribution of SOX9 expression in the distal femoral growth plate. In a highly organized process, proliferating chondrocytes (top) transition to hypertrophic chondrocytes near the metaphysis (bottom). Fibrillar collagen was visualized with second harmonic generation (SHG). The white dotted line marks the transition between cartilage and collagen I/III-rich tissue, corresponding to the increase in SHG signal. This corresponds to the vertical dashed black line in the corresponding profile plots. SOX9 was highly expressed in the proliferative zone and the pre- hypertrophic zone while being absent in the terminal hypertrophic zone, where blood vessels emerged. The normalized fluorescence intensities of EMCN, SOX9 and SHG were spatially quantified along the white arrow confirming that vascular growth into the cartilage zone is inhibited as long as SOX9 expression is high. (star symbol = mineralized area, hash symbol = cartilage) C. Spatial distribution of SPARC expression in the growth plate. The normalized fluorescence intensities of EMCN, SPARC and SHG were spatially quantified along the white arrow showing that the onset of SPARC expression preceded the emergence of blood vessels. The emerging cell population with high SPARC expression in the hypertrophic zone and in mineralized regions, suggests an important role for SPARC in regulating hypertrophic chondrocyte function and bone mineralization. Shown are single plane images from acquired *Z*-stacks. An overview image of the whole femur stained for SPARC can be found in Fig. S1. D, E, F. The growth plate was further stained for nuclei (DAPI), F-actin and fibronectin using a polyclonal antibody. High cellular density was observed on both sides of the growth plate (D). The cartilaginous zone, characterized by proliferative chondrocytes, showed minimal F-actin (E) and fibronectin (F) signal, while actin and fibronectin expression were markedly high behind the hypertrophic zone. This suggests the emergence of osteoblasts. G, H. SHG imaging of fibrillar collagen (G) was superimposed with fibronectin and F-actin staining to spatially quantify their intensity profiles along the white arrow in the merged image. The corresponding intensity profiles crossing the cartilage-bone transition zone revealed that fibronectin assembly preceded collagen fibrillogenesis (H). I, J, K. Zoom-in images revealed SHG signals in the cartilage zone originating from thin collagen II fibers. Consistent with characteristics typical of growth plate cartilage, collagen II fibers were highly organized and aligned along the central bone axis, underscoring the regulated nature of bone growth.

SOX9 and SPARC (Fig. 1B, C). This observation is notable, as SPARC expression has also been implicated in promoting chondrocyte degradation [52]. In the collagen I/III-rich region, as detected by SHG imaging, SPARC was furthermore found in association with the fibrous collagen matrix (Fig. 1C), further supporting its proposed role in promoting collagen fibrillogenesis [53]. An overview image of the entire femur, showing both the distal growth plate and the fracture gap, highlights the high SPARC expression within the endochondral ossification zone of the growth plate (Fig. S1).

2.3. De novo assembly of fibronectin started first in the hypertrophic zone of the growth plate, while collagen I/III fibers appeared in more proximal regions toward the metaphysis

Chondrocyte stacks exhibited a highly organized columnar arrangement within the cartilaginous zone of the growth plate, as expected and confirmed by additional DAPI staining for nuclei (Fig. 1D). DAPI staining further revealed a reduced cell density within the proliferative cartilage zone, compared to the mineralized region toward the metaphysis, due to the high ECM content. This ECM is rich in proteoglycans such as aggrecan, which inhibit cell spreading and contractility. Cell density progressively increased toward the regions of de novo bone formation (Fig. 1D). Proliferative chondrocytes showed minimal F-actin organization, consistent with limited cytoskeletal contractility (Fig. 1E). As cell attachment to the ECM increases, actin polymerization is promoted, enhancing cell contractility [54]. In agreement with this, while very little F-actin was detected within the proliferative cartilage zone, strong F-actin expression was observed proximal to the

hypertrophic zone, extending toward the bone metaphysis (Fig. 1E).

We next analyzed changes in ECM composition during the transition from the proliferative cartilage zone through the hypertrophic zone and into the mineralized region. Since chondrocytes in the hypertrophic zone exhibit increased spreading and cytoskeletal reorganization, we assessed fibronectin distribution across the different zones [55,56]. As expected, fibronectin was absent from the columnar stacks of proliferative chondrocytes within the cartilage zone. In contrast, fibronectin

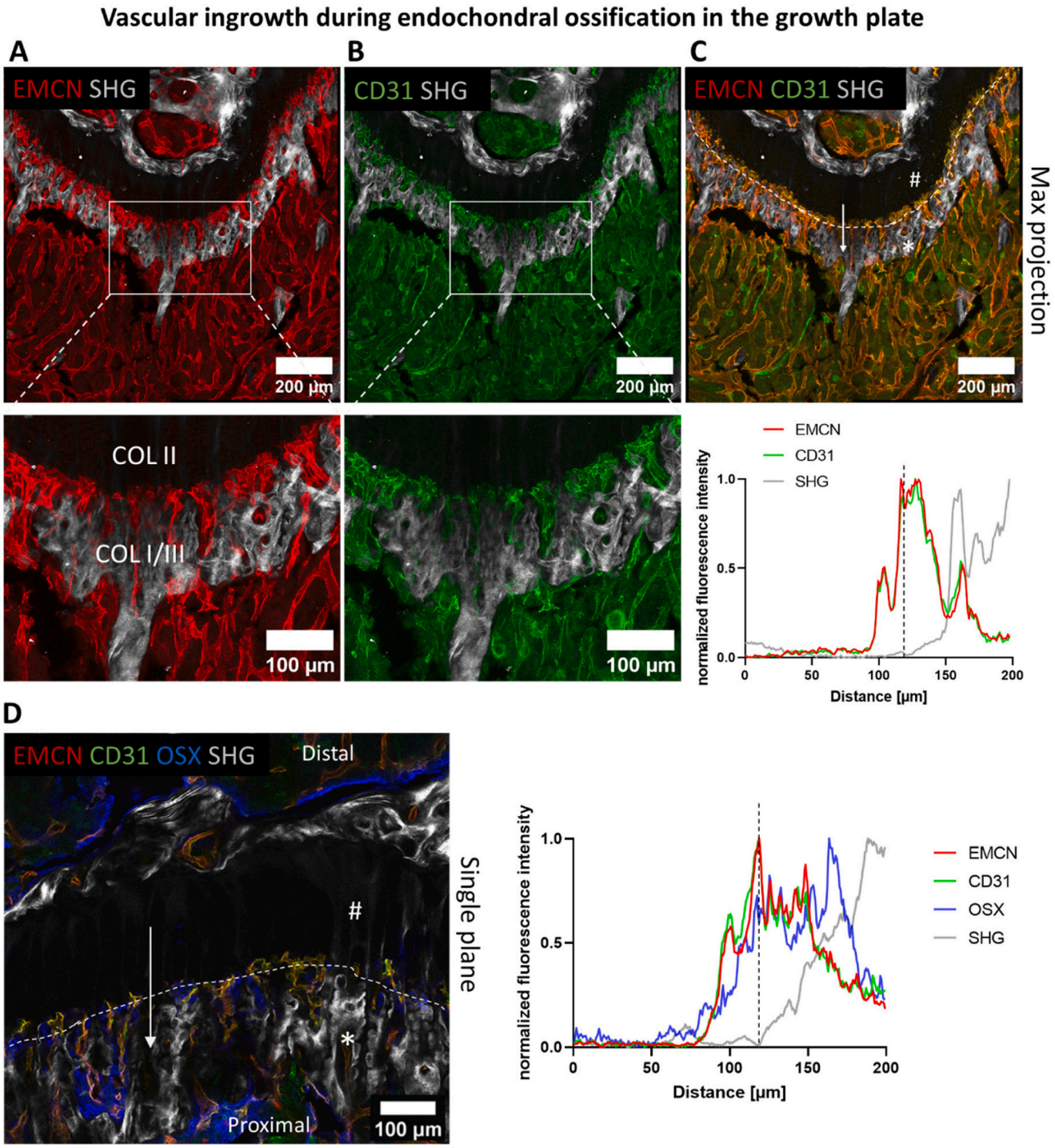

Fig. 2. In the growth plate, blood vessels invaded the hypertrophic cartilage zone, followed by the initial deposition of fibrillar collagen in regions more toward the metaphysis. A-B. Maximum intensity images of EMCN and CD31 along with SHG imaging to assess vascular invasion into the growth plate. Shown are avascular cartilaginous zone of the growth plate (black area) and the interface of cartilaginous zone and bone formation. C. The white dotted line marks the transition between cartilage and collagen I/III-rich tissue, corresponding to the increase in SHG signal observed in the corresponding profile plots, as indicated by the vertical dashed black line. Intensity plots for EMCN, CD31 and SHG along the white arrow crossing the cartilage-bone transition zone revealed that blood vessels emerged before fibrillar collagen toward the active growth plate side, the area rich in fibronectin fibers and F-actin and hence contractile cells. (star symbol = mineralized area, hash symbol = cartilage) D. To investigate the presence of pre-osteoblasts, OSX staining was performed. Single planes from Z-stack images were analyzed to assess their spatial relationship to nearby blood vessels. OSX-expressing cells were located in proximity to blood vessels, but appeared slightly more toward the metaphysis compared to the vascular front when crossing the cartilage-bone transition zone.

fibers were detected in the hypertrophic zone, coinciding with areas of increased F-actin assembly (Fig. 1F). This suggests that the assembly of fibronectin fibers in the hypertrophic region coincides with the transition of chondrocytes to hypertrophy. To investigate collagen fiber assembly, we assessed the distribution of fibrillar collagen across different zones of the growth plate using SHG imaging. As expected, fibrillar collagen I/III, which produces an intense SHG signal, was absent in both the proliferative cartilage zone and the hypertrophic zone (Fig. 1G). Collagen I/III fibrils were detected only beyond the hypertrophic zone, more proximally toward the bone metaphysis. Given that fibronectin serves as a template for nucleating collagen fibril assembly [57], a process regulated by fibronectin fiber tension [58], we tested whether fibronectin deposition preceded the appearance of fibrillar collagen I/III during endochondral ossification in vivo. Indeed, intensity profiles of fibronectin and SHG-positive fibrillar collagen along a selected ROI crossing the cartilage-bone interface demonstrated that fibronectin, along with F-actin, appeared approximately 100 μm more distal compared to the emergence of fibrillar collagen within the hypertrophic zone (Fig. 1H). Since SHG imaging can also capture the much fainter collagen II fibers, which is the main constituent of cartilage, we used SHG imaging to further analyze collagen fiber networks within the proliferative cartilage zone of the growth plate [59,60]. As expected, single plane and zoom-in images revealed the presence of thin collagen II fibers in the cartilaginous proliferative zone (Fig. 1I-K).

2.4. Blood vessel invasion occurred in the hypertrophic zone of the growth plate, followed by the appearance of OSX-expressing cells with spatiotemporal delay

Hypertrophic chondrocytes transition to a pro-angiogenic state, promoting the revascularization necessary for cartilage-to-bone remodeling. To assess the extent of blood vessel invasion into the fibronectin- and F-actin-rich hypertrophic zone, we stained for the typical bone endothelial cell (EC) markers EMCN and CD31, both of which play active roles in coupling angiogenesis to osteogenesis at the growth plate [32]. As expected, the cartilaginous growth plate zone remained avascular, while blood vessels appeared in the hypertrophic zone (Fig. 2A to C). Intensity profiles across a selected ROI spanning the cartilage-bone transition zone revealed that blood vessels (EMCN and CD31) emerged within fibronectin-rich areas, approximately 100 μm more toward the epiphysis compared to the appearance of fibrillar collagen I/III fibers (Fig. 2C). To further assess the onset of ossification, we stained for the transcription factor OSX. OSX-expressing cells were observed aligning along the invading blood vessels, positioned slightly more toward the metaphysis compared to the front of vascular sprouts infiltrating the hypertrophic zone (Fig. 2D). This suggests that vascular sprouts were subsequently followed by (pre-)osteoblasts, which then assembled the collagen I/III matrix and later initiated ossification.

2.5. During early bone fracture healing under semi-rigid fixation at day 7, SOX9 expressing cells were observed centrally within the fracture gap and coincided with blood vessels that invaded from the proximal side

In contrast to the highly organized process of endochondral ossification in the growth plate, chondrogenesis and subsequent endochondral ossification during fracture healing are initiated within a hematoma-filled fracture gap [19]. Understanding how this complex hematoma environment transitions toward chondrogenesis and remodeled into bone remains poorly understood. To investigate this, we employed our well-established mouse osteotomy model using two different external fixation strategies: rigid and semi-rigid stabilization [19]. Since semi-rigid fixation promotes enhanced cartilage formation after 14 days compared to rigid fixation, we selected the semi-rigid condition for our initial analyses. We stained with the same markers as in the growth plate, i.e. for SOX9-expressing chondrocytes and OSX-expressing (pre)osteoblasts, as well as for SPARC, and used SHG imaging to visualize collagen fibers. 7 days after fracture, collagen I/III-rich areas were present at the proximal side of the gap, suggesting already a partially mineralized matrix (Fig. 3A). In contrast, the distal part of the fracture gap, visible as dark areas and indicated by the dashed white line (Fig. 3A), remained filled with hematoma, as previously shown [19]. SOX9 staining to detect the emergence of pre-chondrocytes revealed the absence of SOX9 in collagen I/III-rich areas, while being predominantly expressed further toward the center of the osteotomy gap extending toward the hematoma region (Fig. 3A). Single-plane images from the acquired *Z*-stacks, along with zoomed-in views, revealed the presence of thin collagen II fibers at sites of SOX9 expression (Fig. 3A). This suggests that SOX9-positive cells had already begun assembling a collagen II matrix just beneath the proximal collagen I/III matrix. To further investigate the spatial relationship between these early chondrogenic cells and the vascular network, we employed EMCN staining for blood vessel visualization. Since the early fracture gap is highly infiltrated by platelets and monocytes that both express CD31 [42,43], resulting in high background and limited specificity for ECs when staining for CD31, we used EMCN to ensure more specific detection of blood vessels. EMCN staining revealed SOX9 expression at day 7 within vascularized areas of the collagen II-enriched hematoma regions at the center of the fracture gap (Fig. 3A). A higher-resolution, single-plane image further highlighted the presence of thin collagen II fibers in areas of rich SOX9 expression, which already exhibited a cartilage-like fiber morphology (Fig. S2). Analogous to the endosteal region within the osteotomy gap, the surrounding muscle tissue also showed high vascularization accompanied by SOX9-expressing cells (Fig. S3). While some overlap between SOX9-expressing and OSX-expressing cells was observed, the two populations predominantly occupied distinct regions within the fracture gap (Fig. 3B). This finding aligns with existing literature indicating that regions rich in OSX expression typically show a marked absence of SOX9 expression and vice versa, underscoring the suppressive interaction between the pathways they regulate [61–63]. The slightly more diffuse appearance of OSX staining, compared to the punctate nuclear signal of SOX9, likely reflects the higher cellular density of osteoblasts in specific areas, while some residual background signal may also contribute. In the early stages of fracture healing (day 7), a notable co-localization of SPARC and SOX9-expressing cells was seen in some collagen II-rich areas, while SPARC was also present in regions with collagen I/III as it is involved in promoting osteogenic processes (Fig. 3C). Notably, during the early healing phase, SPARC is expressed by multiple cell types and interacts with platelet-derived growth factor (PDGF) during tissue remodeling [64], indicating that SPARC is not restricted to hypertrophic chondrocytes alone as in the growth plate after 7 days.

2.6. Under rigid fixation at day 7, SOX9 expression occurred within a fully vascularized fracture gap

In contrast to semi-rigid fixation, the osteotomy gap is fully vascularized under rigid fixation by day 7 [19]. To evaluate chondrogenesis under these conditions, we analyzed SOX9 expression within the fracture gap stabilized with a rigid fixator. SOX9-positive cells were predominantly localized on the distal side of the fracture gap, whereas no SOX9 expression was detected within the collagen I/III-rich matrix at the proximal side, as expected (Fig. 4A). Notably, SOX9-expressing chondrocytes co-existed with blood vessels within the remnants of the hematoma. Although some SOX9-positive cells were found near blood vessels, the majority were positioned at greater distances from vascular structures (Fig. 4A). Higher-resolution single-plane SHG imaging further confirmed the organization of fibrillar collagen I/III on the proximal side and the presence of thin collagen II fibers on the distal side, aligned with EMCN-positive vessels (Fig. S4). In contrast to the distribution of SOX9-expressing cells, OSX-positive cells were detected primarily on the proximal side of the fracture gap, closely associated with blood vessels, and were absent on the distal side (Fig. 4B).

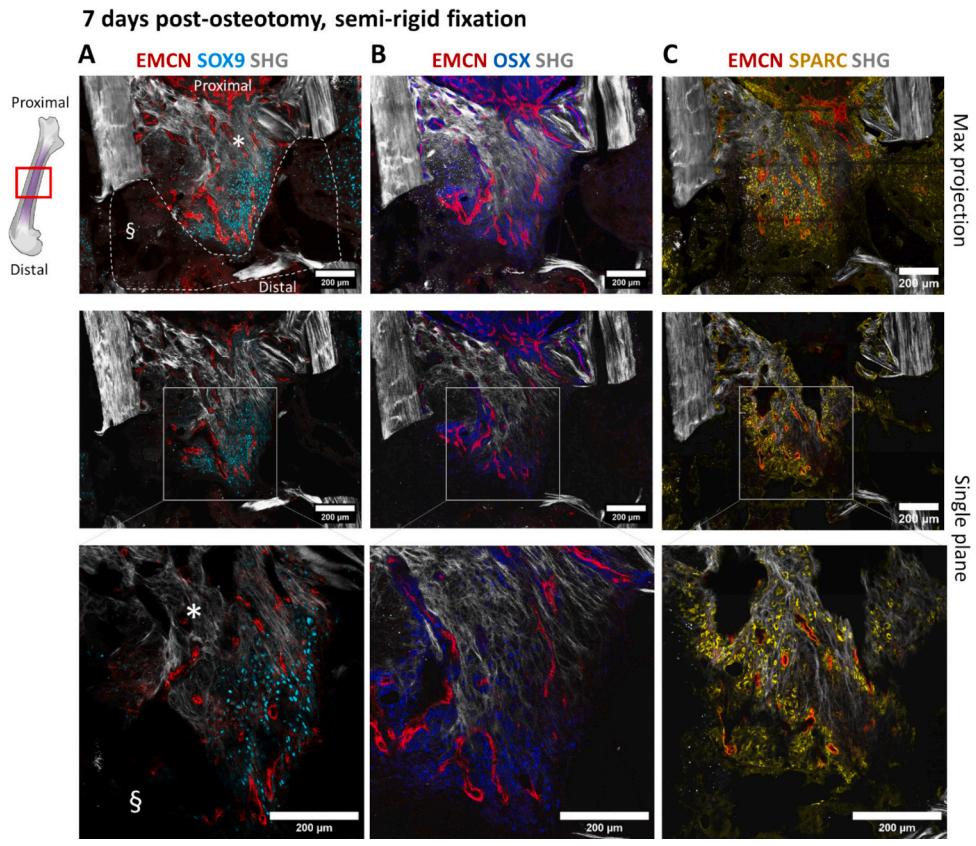

Fig. 3. Spatial distribution of SOX9, SPARC and OSX in the osteotomy gap at day 7 under semi-rigid fixation. Osteotomies were set in 10-week-old female mice on the left femur and the osteotomy gap was stabilized with a semi-rigid fixator. Mice were sacrificed seven days after osteotomy. Fibrillar collagen as visualized using SHG imaging, together with the spatial distribution of SOX9 (A), OSX (B) and SPARC (C) expression. A. SOX9 was expressed below the collagen I/III-rich areas (star symbol), extending toward the avascular hematoma region (dashed white line, paragraph symbol). Zoom-in image revealed the presence of collagen II, identified by a weak SHG signal in regions of SOX9 expression. B. In contrast, OSX was predominantly found in collagen I/III-rich, but also in collagen II-rich areas proximal to the gap, always in close proximity to the blood vessels. C. SPARC was expressed mainly in collagen I/III-rich areas but also co-populated areas together with SOX9-expressing cells.

2.7. External mechanical stability and local vascularization determined the spatial distribution of SOX9- and OSX-expressing cells during fracture healing at day 7

Notable differences in the spatial distribution of SOX9-expressing cells within the fracture gap were observed between fixation types (Fig. 3 and Fig. 4). To further investigate the influence of external mechanical stability on the emergence of SOX9- and OSX-expressing cell populations, we quantified the distances of SOX9-positive cells relative to the proximal fracture end (Fig. 5A) and compared their positions to those of OSX-positive cells. Our analysis revealed that SOX9-expressing cells under rigid fixation were predominantly located further away from the proximal fracture end, whereas under semi-rigid fixation, they located closer to the proximal side (Fig. 5B). In contrast, OSX-positive cells consistently occupied more proximal locations than SOX9-positive cells, regardless of fixation type (Fig. 5B). Because vascularization and oxygen supply are critical factors influencing cellular differentiation [65], we next investigated the spatial relationship between blood vessels and these two cell populations. While mechanical fixation stability is known to modulate overall vascularization during fracture healing, its specific impact on the immediate microenvironment surrounding SOX9- and OSX-positive cells remains unclear. Under both rigid and semi-rigid fixation conditions, higher-magnification images and quantitative analyses confirmed that SOX9-positive cells consistently resided further away from blood vessels than OSX-positive cells (Fig. 5C, D). Together, these findings demonstrate that external mechanical stability regulates vascularization, which in turn shapes the microenvironment and governs the spatial positioning and differentiation of chondrogenic versus osteogenic populations during early fracture healing.

2.8. Under semi-rigid fixation, large avascular collagen II-rich areas, rich in SOX9 and SPARC, connected the proximal and distal bone ends after 14 days

Under semi-rigid fixation after 14 days, the number of SOX9 positive expressing cells had increased significantly compared to the 7-day time point and now localized at the periphery connecting the proximal and distal ends of the fractured bones (Fig. 6A). This phase marks a critical progression in (such a model of delayed) bone healing, in which proliferative chondrocytes promote the development of avascular cartilage tissue, a prerequisite for endochondral ossification now taking place at the bone-cartilage interface (Fig. 6A, zoom-in image). The absence of blood vessels in SOX9 and collagen II-rich areas confirmed that the hematoma still seen at day 7 had been remodeled into avascular cartilage by day 14 (Fig. 6A). In contrast, only a few OSX-expressing cells were found in collagen II-rich cartilage regions. This is in stark contrast to the surrounding tissues, which were rich in OSX expression and blood vessels, originating from the bone marrow and the soft tissue surrounding the bone (Fig. 6B). SPARC-expressing hypertrophic chondrocytes co-existed with SOX9-expressing chondrocytes within the cartilage, but were largely absent in the collagen I/III-rich regions (Fig. 6C). A magnified image from the cartilage-bone interface revealed that blood vessels originating from the OSX-rich region had invaded the

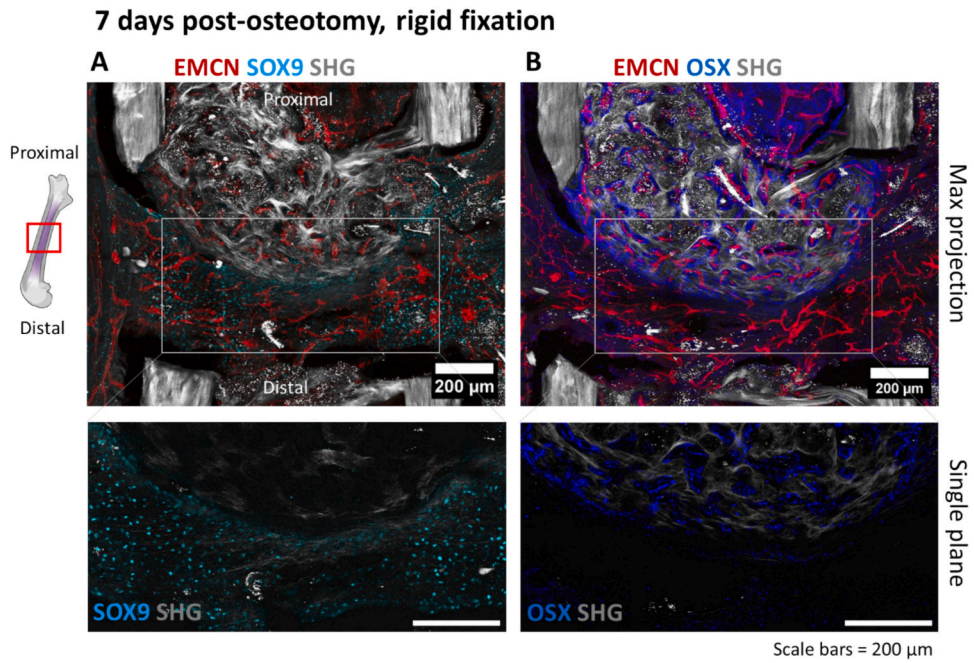

Fig. 4. During the early stages of bone healing under rigid fixation, SOX9-expressing cells co-existed with blood vessels at the distal side of the fracture gap. Osteotomies were set in 10-week-old female mice on the left femur and the osteotomy gap was stabilized with a rigid fixator. Mice were sacrificed seven days after osteotomy. SHG imaging for fibrillar collagen along with SOX9 (A) or OSX (B) staining was performed. A. SOX9-expressing cells were mainly found at the distal collagen II-rich side, but not on the collagen I/III- rich proximal side. Superimposition with EMCN staining for blood vessel visualization revealed SOX9 expression in vascularized areas. Single plane and zoom-in image further revealed SOX9 expression in collagen II-rich distal areas. B. In contrast, OSX-expressing cells were found on the proximal collagen I/III-rich side, while being absent at the distal side.

hypertrophic zone which is a characteristic event preceding bone formation (Fig. 6D). In contrast to the organized chondrocyte alignment observed in growth plate, the faint SHG signal within the osteotomy gap under semi-rigid fixation revealed a disorganized collagen II fibril architecture suggesting that chondrocytes exhibited a multidirectional growth pattern (Fig. 6D).

2.9. Under rigid fixation, avascular SOX9-rich areas only concentrated at the distal tips of the fractured bones after 14 days, thus in previously vascularized areas as found at day 7

Under rigid fixation at day 14, the SOX9 cell population appeared at the tips of the distal fractured bones indicating the rapid build-up of cartilage (Fig. 6E). While these areas were abundant in EMCN positive blood vessels at day 7, they were now depleted of blood vessels (Fig. 6E). The transition of these SOX9-rich areas into avascular zones suggests a process by which vascular structures disappeared as a consequence of chondrogenesis. These blood vessels could disappear due to SOX9-mediated vessel regression [28], with the functional consequence that oxygen levels are expected to decrease in the interior of the chondrocyte condensates, further promoting chondrocyte differentiation and chondrocyte expansion in these areas. At the same time, vessels from the OSX-rich regions invaded the hypertrophic zone of the cartilage tissue indicating bone formation (Fig. 6F, Fig. S5 and Fig. S6). In contrast to semi-rigid fixation, the number of SOX9-expressing cells decreased between day 7 and 14 under rigid fixation (Fig. 6G). This reduction suggests that endochondral ossification and the remodeling of cartilage into bone had begun by day 14, likely initiated by hypertrophic chondrocytes attracting blood vessels, thereby resembling processes observed at the growth plate. Together, these results highlight a critical sequential transition - from an initially vascularized hematoma to an avascular cartilaginous phase, followed by subsequent revascularization - as fundamental stages necessary for successful chondrogenesis and subsequent endochondral bone formation.

3. Discussion

To advance our understanding of the mechanisms governing bone fracture healing, we compared the well-organized progression of chondrogenesis and subsequent endochondral ossification in the growth plate with the complex events observed during fracture repair. Our aim was to explore how chondrogenesis in bone fracture healing is regulated, given that it begins in a disordered environment where the fracture gap is initially filled with a hematoma, triggering a cascade of differentiation and trans-differentiation processes. In contrast, bone growth happens along a linear sequence of cellular differentiation and trans-differentiation steps. We utilized the same cell markers to visualize regions of chondrogenesis and of endochondral ossification in both scenarios. Particular attention was given here to the transcription factors SOX9, as SOX9 is expressed in all cartilage progenitor cells and cartilage except terminal hypertrophic chondrocytes [51], as well as SPARC which is expressed in osteoblasts, but also hypertrophic chondrocytes [34,41] and the osteogenic marker OSX [29].

Within the growth plate, the sequence of events of chondrogenesis followed by endochondral ossification represents the classical form of this biological process. Using this to show how the cell markers used here are differentially expressed during endochondral ossification helps to gain a more fundamental understanding of the process of chondrogenesis and endochondral ossification in bone healing, too. Our study elucidates the spatial distribution of SOX9, SPARC and OSX-expressing cells and highlights their differential dependency on blood vessel proximity, most likely due to alterations in oxygen levels during either chondrogenic or osteogenic differentiation within the growth plate. The organization of SOX9-expressing chondrocytes in stacks within a collagen II-rich matrix (Fig. 1B) reflects the typical architecture of proliferative growth plate cartilage. As the availability of oxygen and other nutrients are diminishing, proliferating chondrocytes gradually became hypertrophic and eventually trans-differentiated into SPARC-expressing osteoblasts [34], which then started to assemble an F-actin rich

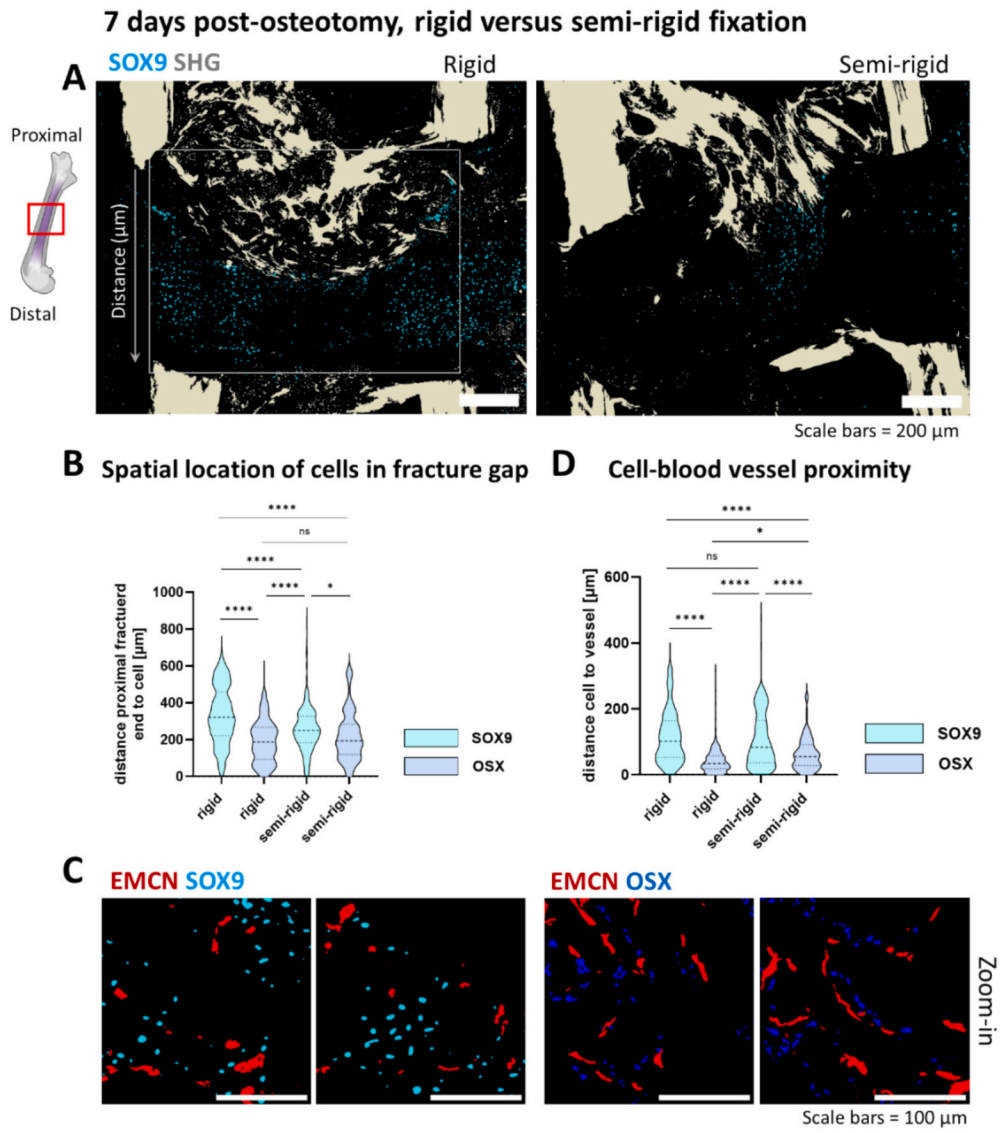

Fig. 5. Comparison of spatial location of SOX9- and OSX-expressing cells in rigid versus semi-rigid fixation and their association with blood vessels. A. Representative rendered images of the osteotomy gap illustrating the distribution of SOX9-expressing cells and fibrillar collagen under rigid and semi-rigid fixation conditions. The fracture gap, outlined as the region of interest (ROI), was used for subsequent quantifications. B. Quantification of cell distances from the proximal fractured end. Violin plots depict the spatial distribution of SOX9- and OSX-expressing cells within the fracture gap across three animals. C. Zoom-in images show the proximity of SOX9-expressing cells compared to OSX-expressing cells in relation to nearby blood vessels. D. Quantitative analysis of the distance between SOX9- and OSX-expressing cells and their nearest blood vessels. Violin plots illustrate distribution of cell proximity to blood vessels within the fracture gap across three animals. Data were compared using a nonparametric Kruskall-Wallis rank test with post hoc Dunn's test for multiple comparisons. * indicates $p < 0.05$, **** indicates $p < 0.0001$.

cytoskeleton concomitant to a fibronectin matrix in the hypertrophic zone (Fig. 1C-F). As long as SOX9 expression is high, hypoxia-induced angiogenesis into the cartilage zone is inhibited, as SOX9 can directly inhibit vascularization by binding to SRY sites within the *Vegfa* gene, thereby repressing its expression [28]. Therefore, the reduction of SOX9 expression in the hypertrophic zone (Fig. 1B), likely enabled the subsequent revascularization to facilitate cartilage-to-bone remodeling. As the SPARC-expressing cell population increased, we propose that increased SPARC release from subchondral osteoblasts further promoted chondrocyte degeneration [52] accompanied by major ECM remodeling. The observed spatial offset between fibronectin and collagen I/III assembly at the cartilage-bone interface - with the latter appearing approximately 100 µm more proximal toward the metaphysis in our model (Fig. 1H) - is to be expected as fibronectin fibers serve as template to nucleate collagen fibrillogenesis [57,58,66]. The continued presence of SPARC in the collagen I/III-rich mineralizing zone is consistent with its documented role in promoting collagen matrix assembly and bone formation [53]. Important to note for our discussion below, chondrogenesis is promoted by reducing the oxygen and nutrient supply, while osteoblast differentiation requires well oxygenated conditions [33,67]. Also a reduced availability of lipids might contribute as this determines the fate of skeletal progenitor cells via SOX9, too [68]. Thus, environmental factors such as oxygen and perhaps other nutrients orchestrate the differential growth versus decline of competing cell populations. Notably, since SOX9-expression is associated with HIF1α signaling, the spatial expression of this marker suggests hypoxic conditions in these areas [31], while OSX expression suggests more oxygenized areas [32,33].

Fracture healing, unlike the structured process observed at the growth plate, starts within a hematoma-filled space, characterized by a co-existing mixture of entrapped cells and others invading from the surrounding tissues. To transform this disordered state into bone over

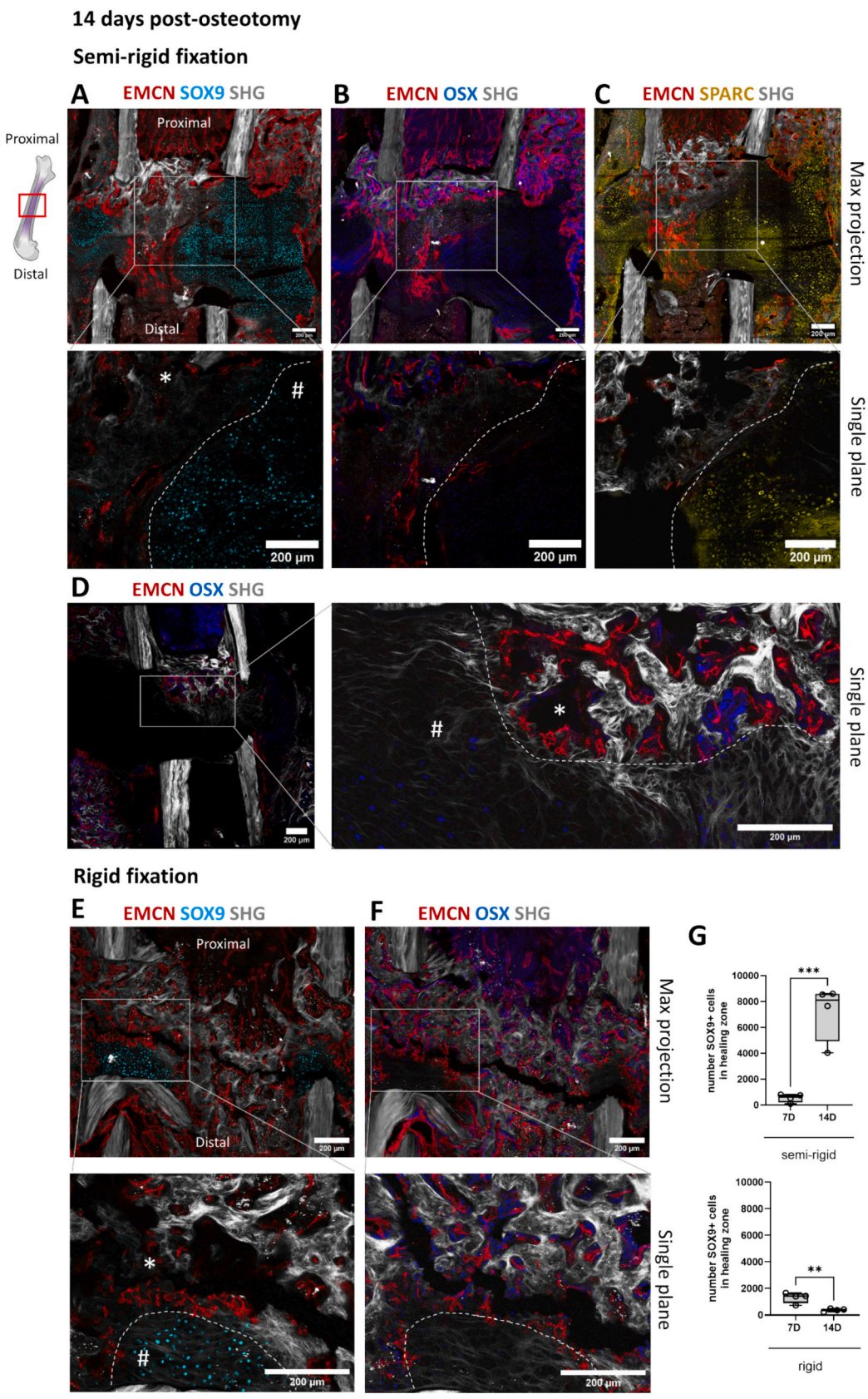

(caption on next page)

Fig. 6. Only under rigid, but not semi-rigid fixation, avascular SOX9-rich regions had emerged in previously vascularized areas at the tips of the distal bone by day 14. Osteotomies were set in 10-week-old female mice on the left femur and the osteotomy gap was stabilized with a semi-rigid or rigid fixator. Mice were sacrificed 14 days after osteotomy. A, B, C. Representative images of the osteotomy gap with fibrillar collagen visualized by SHG imaging and staining of cellular markers SOX9 (A), OSX (B) and SPARC (C) along with EMCN for blood vessel visualization. SPARC-expressing hypertrophic chondrocytes co-existed with SOX9-expressing chondrocytes, while OSX staining revealed minimal OSX expression in SOX9-rich regions, indicating the development of cartilage tissue. Zoom-in images show cartilage-bone interface indicating regions of endochondral ossification (star symbol = mineralized area, hash symbol = cartilage). SOX9 was not expressed in collagen I/III-rich regions, but was highly expressed in collagen II-rich regions. SPARC now showed significantly higher expression in collagen II-rich regions compared to collagen I/III-rich regions. OSX was highly expressed in collagen I/III-rich regions, whereas significantly fewer OSX-expressing cells were observed in collagen II-rich regions. D. Zoom-in and single plane image at the cartilage-bone interface from another sample revealed blood vessel sprouts originating from the OSX-rich region invading the hypertrophic zone of the newly developed cartilage. In contrast to the organized cell stacking observed in the growth plate (Figs. 1 and 2), the chondrocyte matrix within the osteotomy gap showed less organization and exhibited a multidirectional growth pattern. E, F. Representative images of the osteotomy gap 14 days post-osteotomy under rigid fixation, stained for SOX9 (E) and OSX (F) respectively, alongside SHG imaging. Superimposition with EMCN staining for blood vessel visualization revealed the absence of blood vessels in SOX9-rich areas. OSX was highly expressed in collagen I/III-rich regions. Zoom-in images show interface of collagen I/III area (star symbol) and cartilage (hash symbol). G. Quantification of number of SOX9-positive cells in the fracture gap 7 days compared to 14 days post-osteotomy. Significant increase of SOX9-expressing cells in the healing zone from 7 to 14 days under semi-rigid fixation indicating cartilage tissue development. In contrast, rigid fixation resulted in a significant reduction in SOX9-expressing cell numbers at day 14 compared to day 7 ($N = 4$). Statistical analysis using unpaired, parametric *t*-tests was performed. ** indicates $p < 0.01$, *** indicates $p < 0.001$.

time, several processes are at work to orchestrate bone repair with spatiotemporal precision. Using the growth plate to calibrate where to expect the appearance versus disappearance of the cell markers SOX9, SPARC and OSX, we then asked during fracture gap healing where these competing cell populations emerged or disappeared. The spatial locations showing high levels of SOX9 expression within the fracture gap at day 7 were rather different during semi-rigid and rigid fracture fixation. Upon semi-rigid fixation at day 7, chondrogenesis started in the central part of the fracture gap, with additional SOX9-positive cells observed in the surrounding tissue (Fig. S3). The outside-in supply of oxygen and nutrients to the fracture gap is initially facilitated by enhanced erythropoiesis in the bone marrow adjacent to the fracture site in early days [65], followed by enhanced blood vessel ingrowth promoted by hypoxia, and in case of semi-rigid fixation by mechanically driven mass transport. We had previously suggested that the interfragmentary movement might be high enough to supply the hematoma with sufficient oxygen and nutrients via mass transport, driven by gap compression and expansion, such that the onset of angiogenesis is delayed compared to rigid fixation [19]. Our finding that OSX-expressing cells were positioned further from blood vessels under semi-rigid fixation compared to rigid fixation (Fig. 5D) further supports our hypothesis that reduced mechanical stability may alter the local oxygen tension or nutrient gradients within the fracture gap. As cell infiltration and division progress, cell crowding increases, which subsequently reduces the supply of oxygen and nutrients. This reduction, in turn, promotes chondrogenesis in the respective areas. These observations are consistent with the well-known influence of mechanical conditions on fracture healing outcomes: less stable conditions foster greater cartilage formation compared to rigid fixation [20,21,23]. Our data provide a spatial context to this principle, showing that mechanical stability not only affects the amount of cartilage but also its location.

The pronounced SOX9 expression in the center of the fracture gap at day 7 under semi-rigid fixation (Fig. 3A) may indicate that this region is the first to experience reduced oxygen and nutrient availability, likely as movement-induced alterations of shear and compressive forces are least pronounced in the center of the fracture gap. We would like to propose now that, as the emergence of hypoxic conditions is also known to promote the ingrowth of blood vessels, here initiated from the proximal side, we see at day 7 blood vessels in proximity of SOX9-expressing cells in the regions rich in collagen II (Fig. 3A). The finding that areas of SOX9 expression co-exist already with SPARC-rich regions in some areas suggests that these regions are already in the hypertrophic state, in analogy of what is seen for the combination of these markers in the growth plate. As time progressed to day 14, a predominance of SOX9 and/or SPARC-expressing cells is seen in large peripheral avascular regions that were previously filled with avascular hematoma under semi-rigid fixation (Fig. 6A). Chondrogenesis in those areas might got initiated as progressing cell divisions in the limited space, and thus cell jamming, might reduce the mass transport of oxygen and nutrients into these regions. Cell condensation and increasing cell-cell contacts are known to enhance chondrogenesis [69] The combination of markers and their spatial patterning again suggests that these SOX9/SPARC-rich regions at day 14 resembles what is seen in the hypertrophic zone in the growth plate facilitating vascular ingrowth presumably initiated from the proximal side.

Under rigid fixation, after 14 days, initially highly vascularized regions with SOX9-expressing cells had become avascular, but only in regions where cartilage had developed flanking the distal cortices (Fig. 6E). How could this be mechanistically explained? As the blood supply that came mostly from the surrounding soft tissue outside of the bone at day 7, oxygen and nutrient supply might again get reduced due to cell infiltration and division in the hematoma, which might also compress the newly formed blood vessels, as previously observed in tumor tissues [70,71]. Degradation of existing blood vessels might get initiated by SOX9 expressed by chondrocytes at these sites. SOX9 regulates another anti-angiogenic mechanism through Chondromodulin-1 (ChM-1) [72], beyond suppressing the *Vegfa* gene. ChM-1 inhibits EC migration by downregulating proteins such as cyclinD1, cyclinD3, and cdk6. These proteins promote cell division. At the same time ChM-1 upregulates cell cycle inhibitors like $p21^{cip1}$ [73,74]. The upregulated ChM-1 expression may act inhibitory on neighboring ECs [75,76], and may eventually disrupt established endothelial tubes [75,77] and thereby further decrease the oxygen and nutrient supply. As the blood vessels disappeared, the chondrocyte population is taking over other cell populations that require high oxygen levels [78,79], in contrast to chondrogenesis [80]. While vascular regression prior to mesenchymal condensation and chondrogenesis has been studied and confirmed during development [81,82], our study is the first to provide evidence that this process also occurs during bone healing. Similarly, while much attention has been paid to the mechanisms of chondrogenesis and SOX9 during development and within the growth plate [26,51,83,84], their regulation in determining endochondral ossification during fracture repair is less well understood. Altogether, we here propose that the build-up of a chondrogenic cell population proceeds as vessel network structures are actively retracted and disassembled as promoted by an increasing SOX9 expressing cell population. This may progressively create local hypoxic settings necessary to ultimately induce the differentiation to hypertrophic chondrocytes in all those areas that show high SOX9 expression levels at day 7.

Taken together, our findings reveal how the spatiotemporal expression of SOX9- positive chondrocytes, SPARC-positive hypertrophic chondrocytes and osteoblasts, versus OSX-positive osteoblasts orchestrate the events of chondrogenesis and endochondral ossification necessary to heal bone. Using the growth plate to delineate the spatiotemporal synergies of the competing cell populations and their differentiation patterns, we propose a model where blood vessel growth into

the hematoma is followed by a vascular degradation phase which allows chondrogenesis to progress at the tip of the distal bones after 14 days, ultimately leading to vascular regrowth via endochondral ossification at the distal tips of the bone. The observed localized devascularization and the spatiotemporal onset of bone regrowth in the right locations, i.e. at the tips of the distal bones, were evident at day 14 only under rigid fixation. In contrast, semi-rigid fixation did not show localized chondrogenesis at these distal sites. This suggests that tightly regulated vascular remodeling, including transient vascular degradation to facilitate chondrogenesis, is a prerequisite for scar-free healing. Disruption of this sequence may impair endochondral ossification and may contribute to delayed healing or even scarring. Deepening our understanding of these competing processes and how they depend on the mechanical stability of the fracture gap fixation, and how this ultimately relates to scare-free bone regeneration, is of significant medical relevance as they can provide instructions how to promote fracture healing. Particularly the role of interstitial mass-transport as promoted by semi-rigid fixation, and how this interferes with the bone healing processes as observed under rigid fixation, has not been systematically described in the literature or exploited for therapeutic applications.

3.1. Limitations of the study

Limitation of this study include that only snapshots (7d and 14d) were used here to splice together a refined model regarding factors that control the process of chondrogenesis, maturation and finally endochondral ossification, and how it gets well-orchestrated in time and space. Future research could now focus on tracking individual cell populations during the process of fracture healing. This might lead to further insights into trans-differentiation processes beyond of what has already been revealed for hypertrophic chondrocytes [10,85,86], for which it was previously assumed that they would die. Also, other markers or engineered sensors could be utilized to directly measure the oxygen supply with spatiotemporal resolution, as well as of other nutrients necessary to drive the maturation of chondrocytes. Finally, experiments could be designed perhaps using intravital microscopy to study the dynamic process of vascularization. Given the close interplay between vascular and neuronal networks [87], such studies could be expanded to explore neurovascular coupling during callus formation and tissue remodeling. In particular, examining how patterns of neuronal innervation differ between scar-free (rigid) and delayed (semi-rigid) healing conditions may provide further insights into the mechanisms that govern successful healing. While angiogenesis in bone healing has traditionally been viewed as a biphasic process involving hematoma vascularization and endochondral ossification, the intermediate phase requiring devascularization has not been systematically described when studying vascular dynamics. Revealing such a biology-controlled process that induces the vanishing of initially formed angiogenic networks holds promise to design new bioengineering strategies that enable regeneration also in cases and regions where in situ regeneration is challenged. This might also be relevant for therapeutic strategies to treat other angiogenesis-related disorders.

4. Materials and methods

4.1. Mouse osteotomy model to study bone healing versus bone growth

A mouse osteotomy model was used to study both bone healing and bone growth at the growth plate. 10 week old-female mice were used in this study. The experimental procedures were carried out under isoflurane anesthesia, with maintenance through an isoflurane-oxygen mixture administered via a mask. Preoperatively, the animals received a subcutaneous injection of buprenorphine (Temgesic) at a dosage of 0.03 mg/kg while already anesthetized. To prevent intraoperative contamination, prophylactic antibiotic treatment with clindamycin (8 mg/kg body weight) was administered. Surgical interventions were performed on a warming plate to maintain the animals' body temperature. To prevent eye dryness during anesthesia, eye ointment was applied. An external fixator was affixed to the left femur under general anesthesia. This fixator, commercially available (MouseExFix 100 % and 50 %, RISystem), comprises four screws (diameter 0.45 mm) and a radiolucent fixator body. A lateral longitudinal skin incision was made extending from the knee to the hip joint. The iliotibial tract and vastus lateralis muscle were bluntly dissected to expose the femur. Pinholes for external fixator attachment were created using a hand drill, beginning with the first hole just proximal to the distal femoral metaphysis. Three additional pinholes were then drilled to facilitate secure mounting of the external fixator. After securely attaching the external fixator, an osteotomy with a width of 0.7 mm was performed between the two middle pins using a wire saw from RISystem. The wound was closed with layers and animals were returned to their cages with unrestricted mobility and were provided with tramadol in their drinking water (25 mg/L) for pain relief over the following three days. Animals were euthanized 7 or 14 days post-osteotomy under deep anesthesia induced by a ketamine and medetomidine mixture, followed by cervical dislocation. Day 7 was selected to study early healing and hematoma remodeling, while day 14 was chosen to assess endochondral ossification, prior to substantial callus remodeling into mature bone. All statistical analyses were conducted with samples from at least three different litters. Sample processing was blinded until data analysis. Surgeries were performed at the Julius Wolff Institute for Biomechanics and Musculoskeletal Regeneration (LaGeSo G0322/18).

4.2. Rigid versus semi-rigid external fracture fixation as a model system for successful and delayed healing

An external fixation system from RISystem (RISystem AG, Davos, Switzerland) that had previously been established was employed to model successful (rigid fixation) and delayed (semi-rigid fixation) healing. This system allows control of the local mechanical environment at the fracture site as described in detail elsewhere [88,89], and is only briefly summarized here: Rigid fixation facilitates the healing of a 0.5 mm osteotomy gap within three weeks, allowing it to regain mechanical properties comparable to the contralateral intact bone. However, when the fixator is equipped with a semi-rigid fixation bar, it results in doubled shear movements and a substantial increase in shear straining of the tissue, leading to a significant delay in the healing process. Tissue strains under both rigid and semi-rigid fixation conditions were quantified using finite element analysis (FEA) [23]. We previously adapted this model to reflect the 0.7 mm osteotomy gap used in the present study [90]. During the healing process, the initial hematoma transitions into the chondrogenic phase, followed by endochondral ossification and subsequent mineralization. These processes reduce the mechanical strain at the fracture site, ultimately leading to bone bridging between the fracture fragments.

4.3. Bone sample preparation

After euthanasia, femurs were harvested and fixed in 4 % paraformaldehyde (PFA) in PBS for 6–8 h on a shaker. Following PBS washes, the bone samples were transferred to 0.5 M EDTA in H_2O for decalcification and incubated at 4 °C on a shaker for 24 h. After removal of EDTA solution, sucrose solution (20 % sucrose/ 2 % PVP/H_2O) was added and incubated for 6 h at 4 °C on a shaker. Bones were transferred into a cryosection mold and mounted with embedding bone medium (8 % gelatin/ 20 % sucrose/ 2 % PVP in H_2O). Bones were stored at −80 °C. The protocol that we followed has been established previously [91].

4.4. Cryocutting

To prepare cryosections for immunostaining and imaging, cryoblocks were mounted on cryotome sample holder using Tissue-Tek® O.

C.T. Compound (Sakura, # 4583). 50 μm thick sections were cut and directly transferred to glass slides.

4.5. Immunofluorescence staining

Tissue cryosections were thawed, dried for 30 min at room temperature and after rehydration with ice-cold PBS for 5 min samples, permeabilized with ice-cold 0.3 % triton in water for 10 min. Samples were then blocked with 5 % normal serum donkey and 0.3 % triton in 1xPBS for 30 min. Primary antibodies against Fibronectin (Abcam, ab23750, 1:200), EMCN (Santa Cruz, Cat# sc-65,495, 1:100), or CD31/ Pecam-1 (R&D systems, #AF3628, 1:200), or SOX9 (Abcam, [EPR14335–78], ab185966, 1:200), or Sp7/OSX (Abcam, ab22552, 1:200), or SPARC (Abcam, ab203284, 1:200) were diluted in 5 % normal serum donkey in PBS and incubated overnight at 4 °C. Samples were then washed with ice-cold PBS for 5 min three times. Secondary antibodies were diluted in PBS with a 1:200 dilution. Phalloidin-iFluor 488 (Abcam, ab176753, 1:200), which binds to actin filaments, was added for selected tissue sections. For some tissue sections DAPI was added as well. The samples were then incubated with secondary antibody solution for 3 h, followed by washing with PBS and mounting using Fluoromount G (#Cat 0100–01, Southern Biotech). The protocol that we followed for CD31 and EMCN staining has been established previously [91].

4.6. Fluorescence and second harmonic generation imaging of stained tissue sections

Images were acquired using a Leica SP5 confocal microscope. 25 x water immersion objective was used for overview images. Higher resolution images were acquired with 40 x water immersion objective. SHG imaging was used for fibrillar collagen visualization. SHG microscopy is a label-free imaging technique, making it especially well-suited for imaging biological samples [92]. Unlike fluorescence-based techniques, SHG relies on the nonlinear optical interaction between light and tissue-embedded molecules, whereby the SHG signal is generated when two photons interact with a non-centrosymmetric structure and combine to emit a single photon with half the wavelength of the incoming light [93]. Collagen I consist of two α1 chains and one α2 chain arranged in a triple helix, which further assembles into highly ordered fibrils of approximately 20–250 nm, which in turn assemble into fibers of approximately 500 nm [94]. These well-organized, densely packed and non-centrosymmetric fibrillar structures make collagen I fibers highly efficient at generating SHG signals. Additionally, other isoforms, such as collagen III, which plays a role in osteoblastogenesis [44,45], co-localizes with collagen I and thus contributes to the SHG signal. Also, collagen II fibrils, which are predominantly found in cartilage [46], are capable of generating SHG, but at significantly weaker levels. Collagen II is composed of three identical α1(II) chains and forms fibrils that are thinner and less tightly packed than those of collagen I or III [95]. This reduced structural organization results in a much lower SHG signal under equivalent imaging conditions. Therefore, SHG imaging enables to distinguish between collagen I/III-rich bony and collagen II-rich cartilage areas indicated by a comparatively stronger or weaker SHG signal, respectively. An incoming laser wavelength of 910 nm was used for SHG. DAPI was visualized using a multiphoton laser with excitation at 790 nm. *Z*-stacks were acquired for every image. Confocal images were further visualized and analyzed using Fiji (ImageJ) as described below.

4.7. Line profile plots

For profile intensity plots, a custom macro was developed to measure intensity profiles along a selected ROI. Single planes of the maximum intensity projections of acquired image stacks were used. The appearance of the SHG-positive signal at the cartilage-bone transition zone was used as a reference point. This was indicated by the white dashed line in the immunofluorescence images and black dashed line in the corresponding normalized intensity profile plots. Intensity measurements for the respective immunofluorescence signals were taken and the measured data points of the selected ROIs were then transferred to Prism GraphPad, where the profile plots were plotted.

4.8. Analysis of cell distribution, cell-to-blood vessel proximity and number of SOX9-expressing cells

To analyze the spatial distribution of SOX9- and OSX-expressing cells within the fracture gap, binary images of immunostained sections were generated and superimposed with binarized SHG images. A region of interest (ROI) spanning the fracture gap was defined for all samples. Cell distance measurements were performed using Fiji software in combination with a custom-developed macro. This tool quantified the distance of each cell within the gap relative to the proximal fractured cortical end. The resulting distance data for all cells in the gap across samples were visualized as violin plots to assess and compare spatial cell distributions between groups. Similarly, to analyze the proximity of SOX9- and OSX-expressing cells to blood vessels, binarized images of EMCN staining were superimposed with the corresponding binarized cell stainings. The same ROI spanning the fracture gap was applied. Using the same custom Fiji macro, the distance from each cell to the nearest blood vessel was quantified. Proximity data for all cells within the gap were visualized as violin plots to assess and compare spatial proximity of SOX9- and OSX-expressing cells to blood vessels between groups. For quantification of the number of SOX9-expressing cells, the ROI was defined spanning the entire healing zone, including the outer callus at the 14-day time point. Cell quantification was performed using Fiji software in combination with a custom-developed macro that counted the number of SOX9-experssing cells within the healing zone.

4.9. Statistics

Two-tailed paired *t*-tests were conducted using GraphPad Prism software to assess statistical significance between two groups. For comparison between multiple groups displayed as violin plots, the nonparametric Kruskall-Wallis rank test with post hoc Dunn's test for multiple comparisons was applied. Sample sizes are provided in the figure legends. Different *p*-values are indicated by stars in corresponding figures ($*p < 0.05$, $**p < 0.01$, $***p < 0.001$, $****p < 0.0001$).

CRediT authorship contribution statement

Julia Mehl: Writing – review & editing, Writing – original draft, Methodology, Investigation, Conceptualization. **Katharina Schmidt-Bleek:** Writing – review & editing, Methodology. **Agnes Ellinghaus:** Methodology. **Stefan Mundlos:** Writing – review & editing, Investigation. **Holger Gerhardt:** Writing – review & editing, Investigation. **Georg N. Duda:** Writing – review & editing, Writing – original draft, Supervision, Investigation, Conceptualization. **Viola Vogel:** Writing – review & editing, Writing – original draft, Supervision, Investigation, Conceptualization.

Funding

This project was funded by the German Research Foundation within the CRC1444, the Einstein Foundation Berlin and the ERC Advanced Immuno-Mechanics.

Declaration of competing interest

The authors declare no conflict of interest.

Acknowledgments

We thank Mario Thiele for help in developing the macro for intensity profile plots. We further acknowledge Gabriela Korus for her support with histology and Saeed Khomeijani Farahani for help with some of the stainings. We would like to thank Prof. Ansgar Petersen for providing us with fibronectin growth plate stainings from previous studies and initial input.

Appendix A. Supplementary data

Supplementary data to this article can be found online at https://doi.org/10.1016/j.bone.2025.117595.

Data availability

All data necessary to evaluate the conclusions of the paper are included in the main text or in the supplementary materials.

References

[1] K. Mizuhashi, et al., Resting zone of the growth plate houses a unique class of skeletal stem cells, Nature 563 (7730) (2018) 254–258.
[2] P.T. Newton, et al., A radical switch in clonality reveals a stem cell niche in the epiphyseal growth plate, Nature 567 (7747) (2019) 234–238.
[3] B.C. van der Eerden, M. Karperien, J.M. Wit, Systemic and local regulation of the growth plate, Endocr. Rev. 24 (6) (2003) 782–801.
[4] J.C. Lui, Home for a rest: stem cell niche of the postnatal growth plate, J. Endocrinol. 246 (1) (2020) R1–R11.
[5] R.T. Ballock, R.J. O'Keefe, The biology of the growth plate, J. Bone Joint Surg. Am. 85 (4) (2003) 715–726.
[6] P. Kuss, et al., Regulation of cell polarity in the cartilage growth plate and perichondrium of metacarpal elements by HOXD13 and WNT5A, Dev. Biol. 385 (1) (2014) 83–93.
[7] V. Abad, et al., The role of the resting zone in growth plate chondrogenesis, Endocrinology 143 (5) (2002) 1851–1857.
[8] L. Yang, et al., Hypertrophic chondrocytes can become osteoblasts and osteocytes in endochondral bone formation, Proc. Natl. Acad. Sci. USA 111 (33) (2014) 12097–12102.
[9] X. Qin, et al., Runx2 is essential for the transdifferentiation of chondrocytes into osteoblasts, PLoS Genet. 16 (11) (2020).
[10] J.T. Long, et al., Hypertrophic chondrocytes serve as a reservoir for marrow-associated skeletal stem and progenitor cells, osteoblasts, and adipocytes during skeletal development, Elife (2022) 11.
[11] J. Zhu, et al., The role of chondrocyte-to-osteoblast trans-differentiation in fetal bone dysplasia of mice caused by prenatal exposure to dexamethasone, Front. Pharmacol. 14 (2023) 1120041.
[12] R.J. O'Keefe, et al., Analysis of type II and type X collagen synthesis in cultured growth plate chondrocytes by in situ hybridization: rapid induction of type X collagen in culture, J. Bone Miner. Res. 9 (11) (1994) 1713–1722.
[13] L. Wang, et al., SHP2 Regulates the Osteogenic Fate of Growth Plate Hypertrophic Chondrocytes, in Scientific Reports, Nature Publishing Group, 2017.
[14] G.N. Duda, et al., The decisive early phase of bone regeneration, Nat. Rev. Rheumatol. 19 (2) (2023) 78–95.
[15] M. Potente, H. Gerhardt, P. Carmeliet, Basic and therapeutic aspects of angiogenesis, Cell 146 (6) (2011) 873–887.
[16] H. Gerhardt, VEGF and endothelial guidance in angiogenic sprouting, Organogenesis 4 (4) (2008) 241–246.
[17] V. Gebala, et al., Blood flow drives lumen formation by inverse membrane blebbing during angiogenesis in vivo, Nat. Cell Biol. 18 (4) (2016) 443–450.
[18] F. Neto, et al., YAP and TAZ regulate adherens junction dynamics and endothelial cell distribution during vascular development, in: eLife, eLife Sciences Publications Ltd, 2018.
[19] J. Mehl, et al., External Mechanical Stability Regulates Hematoma Vascularization in Bone Healing Rather than Endothelial YAP/TAZ Mechanotransduction, Adv. Sci. (Weinh.) 11 (13) (2024) e2307050.
[20] P. Augat, et al., Mechanics and mechano-biology of fracture healing in normal and osteoporotic bone, Osteoporos. Int. 16 (Suppl. 2) (2005) S36–S43.
[21] H. Schell, et al., The course of bone healing is influenced by the initial shear fixation stability, J. Orthop. Res. (2005) 1022–1028.
[22] J. Lienau, et al., Initial vascularization and tissue differentiation are influenced by fixation stability, J. Orthop. Res. 23 (3) (2005) 639–645.
[23] E. Borgiani, et al., Age-related changes in the mechanical regulation of bone healing are explained by altered cellular mechanoresponse, J. Bone Miner. Res. 34 (10) (2019) 1923–1937.
[24] D.R. Epari, et al., Instability prolongs the chondral phase during bone healing in sheep, Bone 38 (6) (2006) 864–870.
[25] H. Akiyama, et al., The transcription factor Sox9 has essential roles in successive steps of the chondrocyte differentiation pathway and is required for expression of Sox5 and Sox6, J. Bone Miner. Res. 17 (2002) S142.
[26] H. Akiyama, et al., Osteo-chondroprogenitor cells are derived from Sox9 expressing precursors, Proc. Natl. Acad. Sci. USA 102 (41) (2005) 14665–14670.
[27] C.D. Oh, et al., SOX9 regulates multiple genes in chondrocytes, including genes encoding ECM proteins, ECM modification enzymes, receptors, and transporters, PLoS One 9 (9) (2014) e107577.
[28] T. Hattori, et al., SOX9 is a major negative regulator of cartilage vascularization, bone marrow formation and endochondral ossification, Development 137 (6) (2010) 901–911.
[29] Q. Liu, et al., Recent advances of Osterix transcription factor in osteoblast differentiation and bone formation, Front. Cell Dev. Biol. 8 (2020) 601224.
[30] K.M. Sinha, X. Zhou, Genetic and molecular control of osterix in skeletal formation, J. Cell. Biochem. 114 (5) (2013) 975–984.
[31] R. Amarilio, et al., HIF1α regulation of Sox9 is necessary to maintain differentiation of hypoxic prechondrogenic cells during early skeletogenesis, Development 134 (21) (2007) 3917–3928.
[32] A.P. Kusumbe, S.K. Ramasamy, R.H. Adams, Coupling of angiogenesis and osteogenesis by a specific vessel subtype in bone, in: Nature, Nature Publishing Group, 2014, pp. 323–328.
[33] J.C. Utting, et al., Hypoxia inhibits the growth, differentiation and bone-forming capacity of rat osteoblasts, Exp. Cell Res. 312 (10) (2006) 1693–1702.
[34] J.T. Hecht, E.H. Sage, Retention of the matricellular protein SPARC in the endoplasmic reticulum of chondrocytes from patients with pseudoachondroplasia, J. Histochem. Cytochem. 54 (3) (2006) 269–274.
[35] E.M. Rosset, A.D. Bradshaw, SPARC/osteonectin in mineralized tissue, Matrix Biol. 52-54 (2016) 78–87.
[36] T. Hatori, et al., SPARC is a decoy counterpart for c-Fos and is associated with osteoblastic differentiation of bone marrow stromal cells by inhibiting adipogenesis, Mol. Med. Rep. 27 (2) (2023).
[37] Y.A. Choi, et al., Secretome analysis of human BMSCs and identification of SMOC1 as an important ECM protein in osteoblast differentiation, J. Proteome Res. 9 (6) (2010) 2946–2956.
[38] S. Enault, et al., Evolution of dental tissue mineralization: an analysis of the jawed vertebrate SPARC and SPARC-L families, BMC Evol. Biol. 18 (1) (2018) 127.
[39] J.D. Termine, et al., Osteonectin, a bone-specific protein linking mineral to collagen, Cell 26 (1 Pt 1) (1981) 99–105.
[40] T. Sasaki, Crystal structure and mapping by site-directed mutagenesis of the collagen-binding epitope of an activated form of BM-40/SPARC/osteonectin, EMBO J. 17 (6) (1998) 1625–1634.
[41] A.M. Delany, et al., Osteonectin-null mutation compromises osteoblast formation, maturation, and survival, Endocrinology 144 (6) (2003) 2588–2596.
[42] P.J. Newman, The biology of PECAM-1, J. Clin. Invest. 100 (11 Suppl) (1997) S25–S29.
[43] M.J. Metzelaar, et al., Biochemical characterization of PECAM-1 (CD31 antigen) on human platelets, Thromb. Haemost. 66 (6) (1991) 700–707.
[44] E.L. Miedel, et al., Type III collagen modulates fracture callus bone formation and early remodeling, J. Orthop. Res. 33 (5) (2015) 675–684.
[45] S.W. Volk, et al., Type III collagen regulates osteoblastogenesis and the quantity of trabecular bone, Calcif. Tissue Int. 94 (6) (2014) 621–631.
[46] D.R. Eyre, M.A. Weis, J.J. Wu, Articular cartilage collagen: an irreplaceable framework? Eur. Cell. Mater. 12 (2006) 57–63.
[47] H.M. Kronenberg, Developmental regulation of the growth plate, Nature 423 (6937) (2003) 332–336.
[48] S.M. Romereim, et al., A dynamic cell adhesion surface regulates tissue architecture in growth plate cartilage, Development 141 (10) (2014) 2085–2095.
[49] K.L. Cooper, et al., Multiple phases of chondrocyte enlargement underlie differences in skeletal proportions, Nature 495 (7441) (2013) 375–378.
[50] S.A. Hallett, W. Ono, N. Ono, Growth plate chondrocytes: skeletal development, growth and beyond, Int. J. Mol. Sci. 20 (23) (2019).
[51] A. Haseeb, et al., SOX9 keeps growth plates and articular cartilage healthy by inhibiting chondrocyte dedifferentiation/osteoblastic redifferentiation, Proc. Natl. Acad. Sci. USA 118 (8) (2021).
[52] A. Jiang, et al., Increased Sparc release from subchondral osteoblasts promotes articular chondrocyte degeneration under estrogen withdrawal, Osteoarthr. Cartil. 31 (1) (2023) 26–38.
[53] A.D. Bradshaw, The role of SPARC in extracellular matrix assembly, J. Cell. Commun. Signal. 3 (3–4) (2009) 239–246.
[54] A.U. Khan, et al., A glance on the role of actin in osteogenic and adipogenic differentiation of mesenchymal stem cells, Stem Cell Res Ther 11 (1) (2020) 283.
[55] R.O. Hynes, The extracellular matrix: not just pretty fibrils, Science 326 (5957) (2009) 1216–1219.
[56] V. Vogel, Unraveling the mechanobiology of extracellular matrix, Annu. Rev. Physiol. 80 (2018) 353–387.
[57] J. Sottile, et al., Fibronectin-dependent collagen I deposition modulates the cell response to fibronectin, Am. J. Phys. Cell Phys. 293 (6) (2007) C1934–C1946.
[58] K.E. Kubow, et al., Mechanical forces regulate the interactions of fibronectin and collagen i in extracellular matrix, in: Nature Communications, Nature Publishing Group, 2015, pp. 1–11.
[59] A. Nair, et al., Characterization of collagen response to bone fracture healing using polarization-SHG, Sci. Rep. 12 (1) (2022) 18453.
[60] P. Bruckner, M. van der Rest, Structure and function of cartilage collagens, Microsc. Res. Tech. 28 (5) (1994) 378–384.
[61] A.X. Cheng, P.G. Genever, SOX9 determines RUNX2 transactivity by directing intracellular degradation, J. Bone Miner. Res. 25 (12) (2010) 2404–2413.
[62] G. Zhou, et al., Dominance of SOX9 function over RUNX2 during skeletogenesis, Proc. Natl. Acad. Sci. USA 103 (50) (2006) 19004–19009.

[63] L.L. Topol, et al., Sox9 inhibits Wnt signaling by promoting β-catenin phosphorylation in the nucleus, J. Biol. Chem. 284 (5) (2009) 3323–3333.
[64] E.W. Raines, et al., The extracellular glycoprotein SPARC interacts with platelet-derived growth factor (PDGF)-AB and -BB and inhibits the binding of PDGF to its receptors, Proc. Natl. Acad. Sci. USA 89 (4) (1992) 1281–1285.
[65] A. Lang, et al., Local erythropoiesis directs oxygen availability in bone fracture repair, bioRxiv (2025), https://doi.org/10.1101/2025.01.10.632440. https://www.ncbi.nlm.nih.gov/pubmed/39829797.
[66] M.C. Benn, et al., How the mechanobiology orchestrates the iterative and reciprocal ECM-cell cross-talk that drives microtissue growth, Sci. Adv. 9 (13) (2023).
[67] Q. Qin, et al., Hypoxia-Inducible Factors Signaling in Osteogenesis and Skeletal Repair, Int. J. Mol. Sci. 23 (19) (2022).
[68] N. van Gastel, et al., Lipid availability determines fate of skeletal progenitor cells via SOX9, Nature 579 (7797) (2020) 111–117.
[69] B. Cao, et al., Effects of cell-cell contact and oxygen tension on chondrogenic differentiation of stem cells, Biomaterials 64 (2015) 21–32.
[70] T.P. Padera, et al., Pathology: cancer cells compress intratumour vessels, Nature 427 (6976) (2004) 695.
[71] R.K. Jain, J.D. Martin, T. Stylianopoulos, The role of mechanical forces in tumor growth and therapy, Annu. Rev. Biomed. Eng. 16 (2014) 321–346.
[72] A. Takimoto, et al., Direct conversion of tenocytes into chondrocytes by, Exp. Cell Res. 318 (13) (2012) 1492–1507.
[73] H. Mera, et al., Chondromodulin-1 directly suppresses growth of human cancer cells, BMC Cancer 9 (2009) 166.
[74] P. Klinger, et al., Chondromodulin 1 stabilizes the chondrocyte phenotype and inhibits endochondral ossification of porcine cartilage repair tissue, Arthritis Rheum. 63 (9) (2011) 2721–2731.
[75] M. Fujii, et al., Chondromodulin-I derived from the inner meniscus prevents endothelial cell proliferation, J. Orthop. Res. 31 (4) (2013) 538–543.
[76] K. Kusafuka, et al., Cartilage-specific matrix protein, chondromodulin-I (ChM-I), is a strong angio-inhibitor in endochondral ossification of human neonatal vertebral tissues: relationship with angiogenic factors in the cartilage, Acta Histochem. 104 (2) (2002) 167–175.
[77] S. Miura, et al., Impairment of VEGF-A-stimulated lamellipodial extensions and motility of vascular endothelial cells by chondromodulin-I, a cartilage-derived angiogenesis inhibitor, Exp. Cell Res. 316 (5) (2010) 775–788.
[78] S.K. Ramasamy, et al., Blood flow controls bone vascular function and osteogenesis, Nat. Commun. 7 (2016).
[79] F. Diomede, et al., Functional Relationship between Osteogenesis and Angiogenesis in Tissue Regeneration, Int. J. Mol. Sci. 21 (9) (2020).
[80] H.H. Lee, et al., Hypoxia enhances chondrogenesis and prevents terminal differentiation through PI3K/Akt/FoxO dependent anti-apoptotic effect, Sci. Rep. 3 (2013).
[81] M. Yin, M. Pacifici, Vascular regression is required for mesenchymal condensation and chondrogenesis in the developing limb, Dev. Dyn. 222 (3) (2001) 522–533.
[82] R. Hallmann, et al., Regression of blood vessels precedes cartilage differentiation during chick limb development, Differentiation 34 (2) (1987) 98–105.
[83] A.N. Molin, et al., Skeletal growth is enhanced by a shared role for SOX8 and SOX9 in promoting reserve chondrocyte commitment to columnar proliferation, Proc. Natl. Acad. Sci. USA 121 (8) (2024).
[84] V. Lefebvre, M. Dvir-Ginzberg, SOX9 and the many facets of its regulation in the chondrocyte lineage, Connect. Tissue Res. 58 (1) (2017) 2–14.
[85] L. Yang, et al., Hypertrophic chondrocytes can become osteoblasts and osteocytes in endochondral bone formation, in: Proc. Natl. Acad. Sci. U. S. A, National Academy of Sciences, 2014, pp. 12097–12102.
[86] K. Wang, et al., The emerging role of cell transdifferentiation in skeletal development and diseases, Int. J. Mol. Sci. 23 (11) (2022).
[87] P. Carmeliet, M. Tessier-Lavigne, Common mechanisms of nerve and blood vessel wiring, Nature 436 (7048) (2005) 193–200.
[88] B. Kruck, et al., Sclerostin neutralizing antibody treatment enhances bone formation but does not rescue mechanically induced delayed healing, J. Bone Miner. Res. 33 (9) (2018) 1686–1697.
[89] R.M. Hoerth, et al., Correlations between nanostructure and micromechanical properties of healing bone, J. Mech. Behav. Biomed. Mater. 77 (2018) 258–266.
[90] C. Dazzi, et al., External mechanical loading overrules cell-cell mechanical communication in sprouting angiogenesis during early bone regeneration, PLoS Comput. Biol. 19 (11) (2023) e1011647.
[91] A.P. Kusumbe, et al., Sample preparation for high-resolution 3D confocal imaging of mouse skeletal tissue, Nat. Protoc. 10 (12) (2015) 1904–1914.
[92] P.J. Campagnola, L.M. Loew, Second-harmonic imaging microscopy for visualizing biomolecular arrays in cells, tissues and organisms, Nat. Biotechnol. 21 (11) (2003) 1356–1360.
[93] L. Mostaco-Guidolin, N.L. Rosin, T.L. Hackett, Imaging collagen in scar tissue: developments in second harmonic generation microscopy for biomedical applications, Int. J. Mol. Sci. 18 (8) (2017).
[94] D.J. Hulmes, Building collagen molecules, fibrils, and suprafibrillar structures, J. Struct. Biol. 137 (1–2) (2002) 2–10.
[95] M.D. Shoulders, R.T. Raines, Collagen structure and stability, Annu. Rev. Biochem. 78 (2009) 929–958.